Surface & Coatings Technology 204 (2010) 3729–3737

Contents lists available at ScienceDirect

Surface & Coatings Technology

journal homepage: www.elsevier.com/locate/surfcoat

Inactivation of *E. coli* and *B. subtilis* by a parallel-plate dielectric barrier discharge jet

M.H. Chiang [a], J.Y. Wu [b], Y.H. Li [b], J.S. Wu [a,*], S.H. Chen [c], C.L. Chang [d]

[a] Department of Mechanical Engineering, National Chiao Tung University, Hsinchu 30010, Taiwan
[b] Department of Bioindustry Technology, Da Yeh University, Changhua 51591, Taiwan
[c] Physics Division, Institute of Nuclear Energy Research, Longtan 32546, Taiwan
[d] Department of Environmental Engineering and Health, Yuanpei University of Science and Technology, Hsinchu 30015, Taiwan

ARTICLE INFO

Article history:
Received 19 January 2010
Accepted in revised form 23 April 2010
Available online 29 April 2010

Keywords:
Atmospheric-pressure plasma
DBD
E. coli
B. subtilis
Survival rate
Distorted sinusoidal voltage

ABSTRACT

Inactivation of *Escherichia coli* and *Bacillus subtilis* using the jet region of a parallel-plate air dielectric barrier discharge (DBD) driven by a distorted sinusoidal voltage power supply under atmospheric-pressure condition is reported. Various types of working gases, including pure N_2, pure O_2, and compressed air, were tested. Discharges were characterized electrically by measuring the discharge current, applied voltage and absorbed power, and optically by measuring the optical emission spectra in the UV–visible range and absorption spectra in the IR range. Results of survival rate show that both *E. coli* and *B. subtilis* cells (up to 10^7 CFU/mL) can be effectively inactivated using less than 18 passes (1.8 s of residence time in total) of exposure to the post-discharge jet region of compressed air and oxygen discharges at different treating distances in the range of 4–20 mm. Among these, the compressed-air discharge performs the best in inactivating both two types of the bacterial cells, because of the abundant ozone generation and probably through the assistance of nitrous oxide generated in the discharge. In summary, the post-discharge jet region of an oxygen-contained parallel-plate DBD driven by a distorted sinusoidal voltage power driven is very effective in inactivating both *E. coli* and *B. subtilis* cells under the present test conditions.

1. Introduction

Effective sterilization/inactivation of microorganisms is important in maintaining good quality of life for human beings. It is based on either physical or chemical process that destroys or eliminates microorganisms, or both. Conventional sterilization technologies, such as autoclaves, ovens, chemicals such as ethylene oxide (EtO), and radiation (gamma rays) [1,2], heavily rely on irreversible metabolic inactivation or breakdown of vital structural components of microorganisms. Although some of these methods which apply direct heating may be effective in inactivate microorganisms, it is often highly inefficient in terms of time and cost (high energy consumption). Moreover, the use of high-temperature heating stream is often detrimental to some medical products and foodstuffs [3] which are made of heat-sensitive plastics. In addition, the methods which apply radiation are often highly harmful to the human beings who utilize them. Thus, development of a new sterilization technology which is free of the above outstanding problems is important in the bio-medical field.

Sterilization/inactivation using non-thermal plasmas represents one of the promising technologies. Most applications of the plasma technology for sterilization/inactivation require the direct contact of the discharge with the bacterial cells [4], because abundant chemically active ions, electrons and radicals exist in the discharge. The use of low-pressure plasma may be helpful, in which the electrode distance can be quite large. Larger space between electrodes in the low-pressure plasmas means easier handling of the treated bacterial cells, as compared to those using atmospheric-pressure plasmas [5,6], in which the electrode distance is very small (order of mm). However, handling of the test pieces requires the break of vacuum, which is costly. In addition, creation of low-pressure plasmas requires the use of vacuum equipment, which is very expensive and relatively impractical in bio-medical applications.

Recently, sterilization/inactivation using non-thermal atmospheric-pressure plasmas (APPs) has attracted tremendous attention [7,8]. Major advantages of applying atmospheric-pressure plasmas may include [9]: (1) generating abundant bactericidal active agents (chemically active radicals, high kinetic energy ions, electrons, and UV photon), (2) producing fairly low-temperature gas stream which is in direct contact with the bacteria or container, (3) shorter operating time in the order of seconds or minutes, (4) easy removal of the inactivated bacteria and viruses on the treated surface through jet gas stream, and (5) producing essentially no hazardous substances, among others.

Thus, use of the post-discharge jet region of atmospheric-pressure plasma may possibly resolve this dilemma, although the corresponding plasma density is expected to be lower than that in the discharge. However, use of the post-discharge region can render

* Corresponding author. EE425, 1001 University Road, Hsinchu 30010, Taiwan. Tel.: +886 3 573 1693; fax: +886 3 611 0023.
E-mail address: chongsin@faculty.nctu.edu.tw (J.S. Wu).

0257-8972/$ – see front matter.
doi:10.1016/j.surfcoat.2010.04.057

the plasma source a stand-alone module, which could be possibly used for sterilizing/inactivating surfaces that may contain bacterial cells. It is thus the major goal of this paper to study the effectiveness of the post-discharge jet region of atmospheric-pressure plasma in inactivating typical bacterial cells.

In the present study, we have applied a parallel-plate dielectric barrier discharge (DBD) atmospheric-pressure plasma jet (APPJ) which was driven by a high-voltage distorted sinusoidal voltage power supply to inactivate two typical bacterial cells including *Escherichia coli* and *Bacillus subtilis* in the post-discharge jet region. Various inexpensive working gases including pure N_2, pure O_2, and compressed air were tested and discharges were characterized accordingly.

2. Experimental methods

2.1. Experimental facility

Fig. 1 illustrates the schematic diagram of a parallel-plate DBD atmospheric-pressure plasma jet (APPJ) along with gas supply system and the instrumentation for voltage and current measurements. This APPJ consists of two parallel copper electrodes ($50\times50\times8$ mm each) with embedded cooling water. Each electrode is covered with a ceramic plate in the size of $70\times70\times2$ mm. The dielectric plates are 5 mm extruded from the end of the electrodes (in the flow direction), which can prevent the electrode assembly from arcing. Distance between the two dielectric plates (ceramic) was kept as 1 mm throughout the study. The assembly of electrodes and dielectrics were then covered by an insulation layer made of Teflon to provide safety and prevent arcing problem during operation. This DBD assembly was powered by a distorted sinusoidal voltage power supply (Model Genius-2, EN Technologies Inc.). This power supply facilitates adjustment of frequency (20–60 kHz), power density (low/middle/large), peak current (max. 4A), peak voltage (max. 15 kV), and power (max. 2 kW). Resulting output voltage waveform of the power supply produces the voltage increase, which can possibly enhance the plasma properties. Various working gases flow between the parallel plates include N_2 (99.99%), O_2 (99.99%), and compressed air (produced from an oil-less compressor). The flow rates were controlled by manually adjustable flowmeters. The gas was introduced through two holes at the top of the parallel-plate assembly and then passes through a sieved aluminum plate containing 480 holes (0.5 mm in diameter each) for pressure redistribution, followed by a convergent section with length of 10 mm to coincide with the channel gap size (1 mm) at the end of the section.

2.2. Experimental instrumentation

Input voltage and output current waveform across the electrodes of the parallel-plate discharge were measured by a Rogowski coil (IPC CM-100-MG, Ion Physics Corporation Inc.) and a high-voltage probe (Tektronix P6015A), respectively, through a digital oscilloscope (Tektronix TDS1012B). For the measurement of Lissajous figure (Q–V characteristics) of the discharge, a capacitor with capacitance $C_m = 6.8$ nF and a voltage probe (Tektronix P2220) were used. The optical emission spectral intensity of the APPJ was measured using a monochromator (PI Acton SP 2500) with a Photomultiplier tube (Hamamatsu R928). The infrared spectrum absorbance of the APPJ was measured using an FTIR spectrometer (Bruker Tensor 27). In addition, the morphologies of the bacteria were observed by a scanning electron microscopy (Hitachi S-470 type II). For the clarity of presentation, all the results presented in this paper were performed

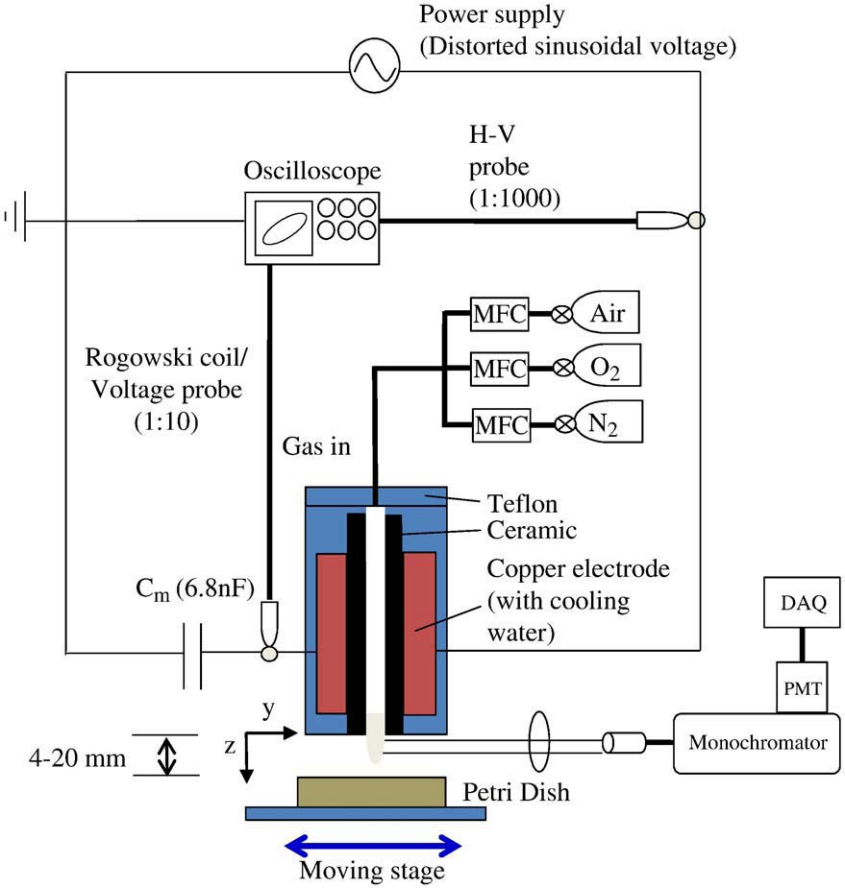

Fig. 1. Sketch of parallel-plate DBD APPJ.

under the condition of 30 kHz (power supply) and 10 slm (flow rate). The Petri dish which contains the bacteria was transported by a pre-programmed moving stage. For the treatment of bacteria, the distance between the bottom edge of the planar DBD and the bacteria was varied in the range of $z = 4$–20 mm. Note "z" denotes the coordinate in the downstream direction measured from the bottom edge of the DBD assembly. The moving speed of the Petri dish was kept as 1 cm/s and number of passes which the DBD jet pass was varied in the range of 1–9. Note "a pass" is defined to be the motion which the APPJ has traveled once over the Petri dish. Resulting residence time over the Petri dish is 0.1 s for a pass under the designated speed. In addition, the gas temperatures in the post-discharge jet region were measured using a K-type thermocouple, which is fixed on a moving stage.

2.3. Sample preparation of bacterial cells

Escherichia coli (BCRC 13014) and *B. subtilis* (BCRC 14716) cultures were grown in 100 mL of Nutrient Broth which was maintained for 12 h and 18 h at 37 °C, respectively. This allowed the cells to reach the exponential-log phase. Cells (10 mL) were harvested and transferred from the broth under sterile conditions to the phosphate buffer solution (90 mL and pH 7.0). The solution was then diluted further continuously to the required concentration level (3.2×10^7 CFU/mL), which is very high as compared to previous studies (e.g., [8]). Then, add 0.1 mL diluted solutions to sterile Petri dishes (diameter 80 mm) containing 20 mL of Nutrient Agar and spread it on the central area of the Petri dishes (4 cm × 4 cm) to make sure all bacteria were treated by the plasma jet with 5 cm in width. During the bacteria preparation we have carefully made sure the Petri dish is properly leveled. Otherwise, some bacteria will flow out of the central area of the Petri dish. The Petri dishes with Nutrient Agar were exposed to the parallel-plate DBD APPJ following the planned test conditions as shown later. After the plasma jet treatment, the Petri dishes were incubated at 37 °C for 24 h, prior to determining the resulting number of colony-forming units (CFU/mL) by NIH ImageJ [10]. This software can easily calculate the area of grown bacteria based on pixel counting, which results in the survival rate of the bacteria in the Petri dish.

2.4. SEM observation

The bacteria of the controls and the plasma-treated samples were rinsed with distilled water and fixed with 2.5% glutaraldehyde solution overnight. The fixed bacterial cells were dehydrated in a graded series of acetone concentration and then dried in a CO_2 atmosphere (HCP-2, Hitachi, Japan) under critical conditions, and then coated with a thin layer of gold. The effects of plasma treatment on the structures of the bacteria were examined using a scanning electron microscopy (Hitachi S-470 type II).

3. Results and discussion

3.1. Electrical properties of the DBD

Fig. 2a–c show the typical measured distorted sinusoidal voltage (30 kHz) input voltage to the electrodes and discharge current waveforms produced in the DBD using pure N_2, pure O_2, and compressed air of 10 slm, in which the output power from the power supply is kept constant (300 W). It is clear that the discharge of N_2 (Fig. 2a) was nearly homogeneous based on the current waveform, while those of pure O_2 (Fig. 2b) and compressed air (Fig. 2c) were filamentary. These can also be further verified from Fig. 5, which illustrates a series of discharge images of these gases. In the first half cycle, current increases rapidly as the gap voltage exceeds the breakdown voltage of gas, but decreases rapidly well before the voltage reaches the peak and crosses the zero current point (thus changes the current direction) as the voltage reaches the peak value. The rapid decrease

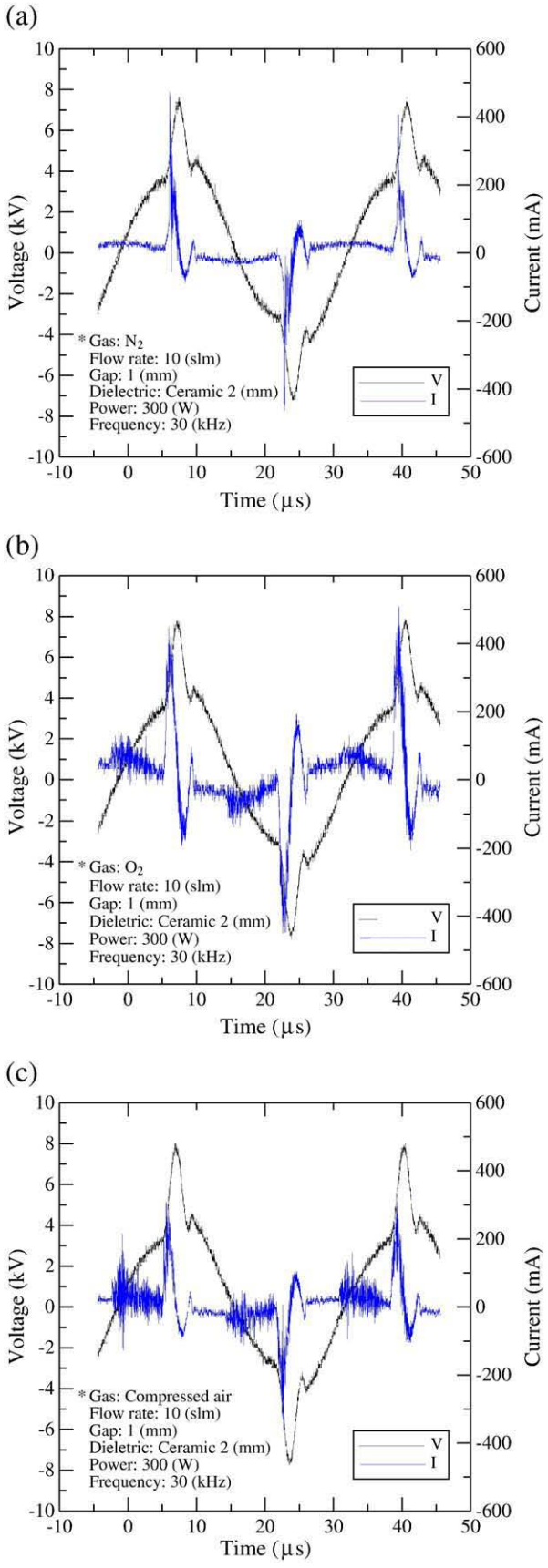

Fig. 2. Typical current and voltage waveforms for various gas discharge. (a) N_2, (b) O_2 and (c) compressed air.

of the current is caused by the extinction of the discharge due to shielding (or memory) effect of the negative surface charge accumulation (electrons) on the dielectric surface, which is a fundamental and well-known mechanism of the DBD that prevents the discharge from arcing. Measured peak current is approximately 400 mA for 25 cm^2 of discharge area, which is equivalent to ~16 mA/cm^2. Earlier one-dimensional fluid modeling for nitrogen DBD driven by sinusoidal voltage waveform [11] has shown that it is a Townsend-like discharge, in which the electron number density is much less than that of ion number density (N_2^+ and N_4^+). Discharges using pure O_2 and compressed air are more filamentary than pure N_2 discharges, as confirmed from the rapid oscillating currents in Fig. 2b and c, and images of microdischarge in Fig. 3.

Fig. 3 shows the bottom view of discharge region, it were taken after 0.2 s of imaging, looking from the downstream side of the parallel plate for N_2, O_2, and compressed-air plasmas. The image of nitrogen discharge looks very bright and uniform in blue color, which is mainly caused by the fluorescence of short-lived excited nitrogen ($N_2(B^3\prod_g)$ and $N_2(C^3\prod_u)$) [12]. The oxygen plasma is a typical electronegative discharge whose image is much darker than other gas discharges that contain nitrogen. In addition, the microdischarges are clearly seen in the images of compressed and oxygen discharge, which are essentially filamentary. This also results in rapid oscillating discharge currents as observed in Fig. 2b and c.

Fig. 4 shows the typical Lissajous figure obtained for the same test conditions as in Fig. 2. The shape of the Q–V curve is a distorted version of the standard parallelogram [13] observed in a DBD driven by a sinusoidal AC power source. When the voltage reaches the peak value (~8 kV), the maximal effective charge (~400 nC) across the electrodes is obtained, which extinguishes the discharge (zero current), as observed in Fig. 2. As the voltage continues to decrease, the effective charge begins to decrease as expected. The electrical energy consumed per voltage cycle E and the plasma absorbed power P can be estimated by the following relations [13]:

$$E = \oint V(t)\mathrm{d}Q \equiv \text{area of } (Q-V)\,\text{diagram} \tag{1}$$

$$P = \frac{1}{T}E = fE \tag{2}$$

where f is the frequency of distorted sinusoidal voltage. Thus, for the corresponding N_2, O_2 and compressed-air discharges, the estimated absorbed plasma power is 88.6 W (28%), 86.4 W (28.8%) and 83.5 W (27.8%), respectively, where the percentage in each parenthesis represents the ratio of absorbed power to input power. Note the input power is directly read from the power supply.

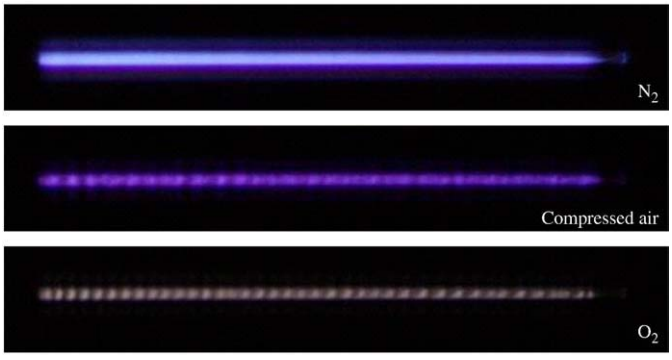

Fig. 3. Bottom view of discharge region for N_2, compressed-air and O_2 discharges. Other discharge parameters are: gas flow rate = 10 slm, power = 300 W, and gap = 1 mm.

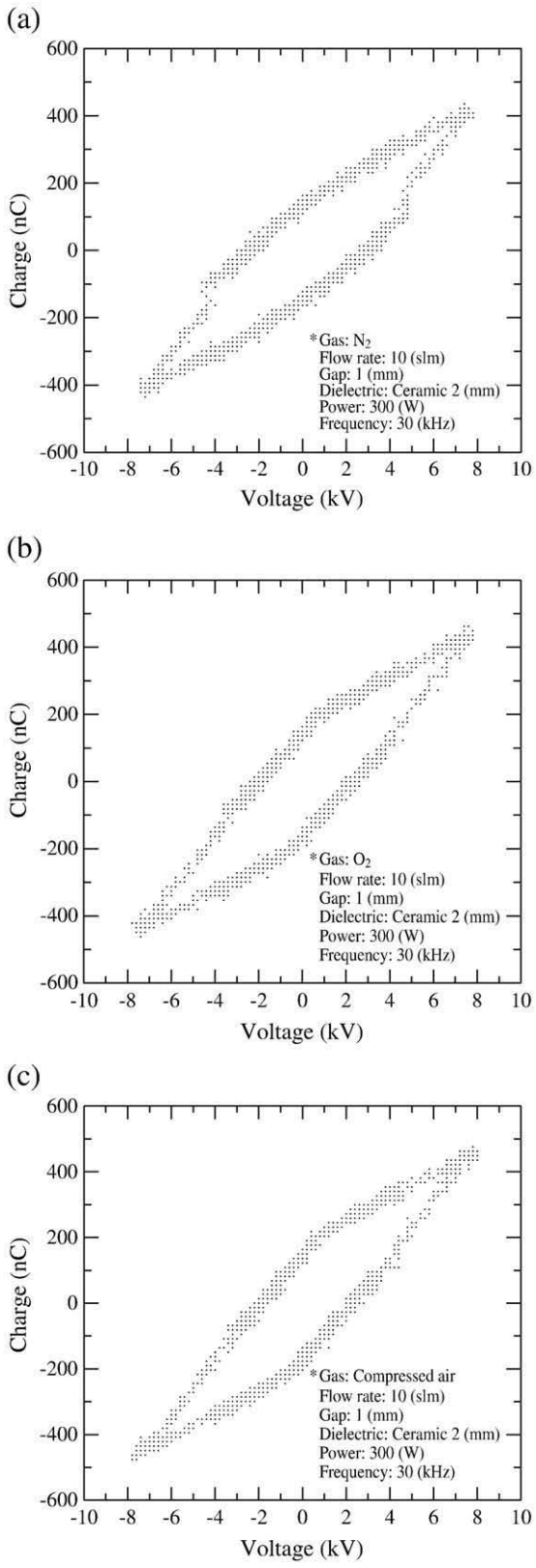

Fig. 4. Lissajous figure for a parallel-plate DBD APPJ in various gas discharge driven by a distorted sinusoidal voltage power supply (30 kHz). (a) N_2, (b) O_2 and (c) compressed air.

Fig. 5 shows the measured gas temperature distribution along the centerline (z = 3–20 mm) (i.e., 8–25 mm from the end of the electrodes) in the post-discharge jet region for N_2, O_2, and compressed-

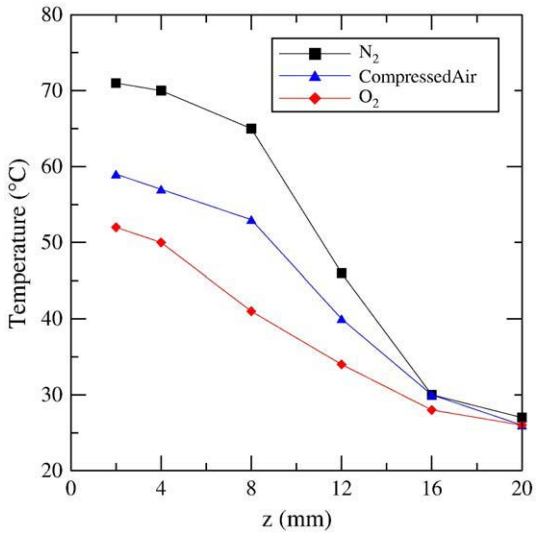

Fig. 5. Temperature distributions in the post-discharge jet region of N_2, Compressed-air and O_2 discharges.

air discharges. Results show that gas temperatures for all the cases decrease rapidly in the downstream direction. For example, the temperature of pure nitrogen case drops from 71 °C ($z=3$ mm) down to 27 °C ($z=20$ mm), which is essentially at room temperature. In addition, gas temperatures for the APPJ containing more nitrogen are higher than those containing more oxygen. This should be attributed to the higher breakdown voltage of nitrogen as compared to that of oxygen. In general, the low gas temperatures in the plasma jet region observed in this study is highly suitable for inactivating bacterial cells without the danger of damaging bio-medical devices.

Fig. 6 shows the side view of the post-discharge region for N_2, O_2, and compressed-air discharges. For the pure nitrogen case, the colorful plume is ~1.5 cm in length having yellow to orange color, which is mainly caused by the fluorescence of the N_2 1st positive lines metastable nitrogen $N_2(B^3\prod_g) \rightarrow N_2(A^3\sum_u^+)$ (500–700 nm). For the discharges generated by pure oxygen and compressed air, the plumes were hardly visible because most of the metastable nitrogen were quenched by the oxygen. In addition, the color can be clearly confirmed from the OES measurements, as typically shown in Fig. 7, which is described in detail next.

Fig. 7 shows the optical emission spectra in the UV and VIS regions measured in the post-discharge region. UV emission is greatly reduced because of the strong electronegativity of O_2 gas, as mentioned earlier. Detailed plasma chemistry is worthy of studying

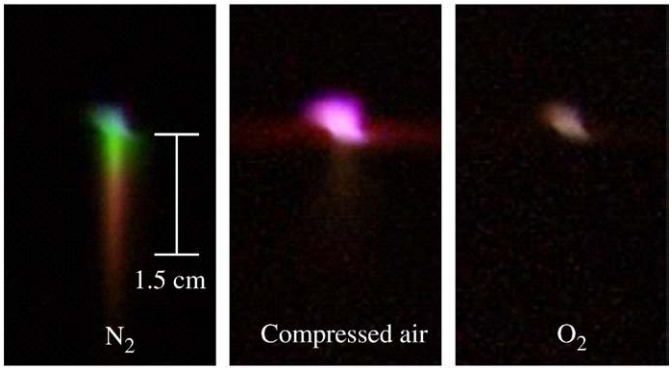

Fig. 6. Side view of post-discharge region for N_2, compressed-air and O_2 discharges. Other discharge parameters are: gas flow rate = 10 slm, power = 300 W, and gap = 1 mm.

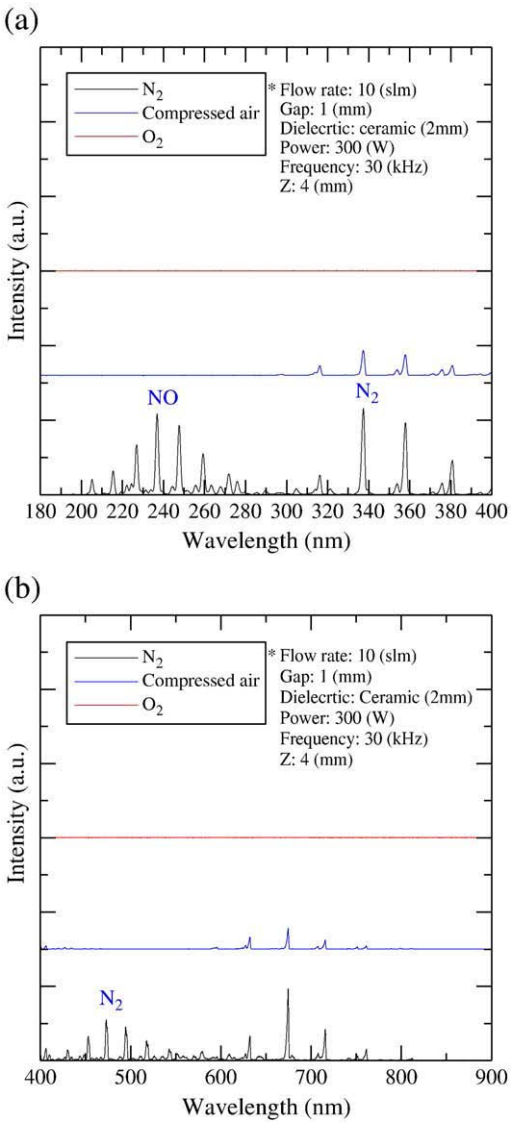

Fig. 7. Optical emission spectrum in the (a) UV and (b) VIS regions for the post-discharge plasma.

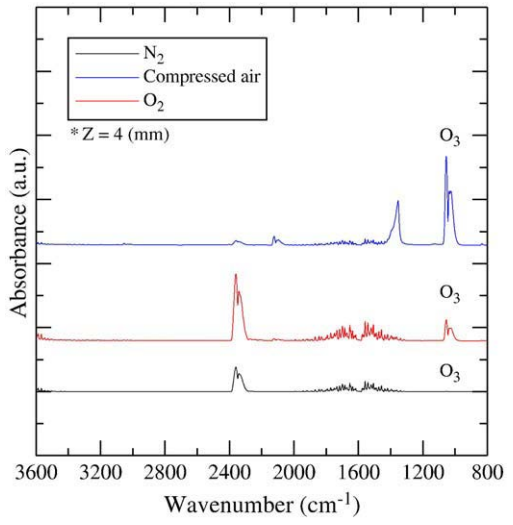

Fig. 8. The infrared spectrum of post-discharge region for N_2, compressed-air, and O_2 discharges in the 800–3600 cm^{-1}.

Table 1
The absorption peak value of 1055 cm^{-1} for ozone in the post-discharge region for N_2, compressed-air, and O_2 discharges in z distance 4–20 mm.

z distance (mm)	N_2 plasma	Compressed-air plasma	O_2 plasma
4	0.00017	0.032	0.138
8	0.00037	0.033	0.135
12	0.0004	0.028	0.14
16	0.00001	0.0188	0.104
20	0.00001	0.0152	0.083

using more detailed measurements or simulations in the near future. In addition, in the range of 450–550 nm, emission of nitrogen discharge is much stronger than those of pure oxygen and compressed-air discharges, which causes the yellow–orange plume as observed in Fig. 6.

Fig. 8 shows the infrared absorption spectra of post-discharge region for N_2, O_2, and compressed-air discharges in the 800–3600 cm^{-1} as measured by in-situ FTIR technique. Strong absorption peak of 1055 cm^{-1} for ozone was clearly observed in compressed-air and O_2 discharges because of abundant oxygen species in the discharges. Note ozone was generated in the discharge and was carried downstream since ozone is relatively long lived. Table 1 shows the absorption peak value of 1055 cm^{-1} for ozone in the post-discharge region for N_2, compressed-air and O_2 discharges in the range of $z = 4$–20 mm. Results show that very high level of ozone can be produced in the post-discharge region of compressed-air and oxygen cases. Observed abundant ozone plays a key role in the inactivation of bacteria cells that is described next.

3.2. Inactivation of *E. coli* and *B. subtilis*

In the current study, the number of *E. coli* and *B. subtilis* on each Petri dish was controlled as ~10^7 CFU/mL, respectively, before plasma jet treatment. Figs. 9 and 10 show the appearance of the Petri dish for *E. coli* and *B. subtilis*, respectively, after incubation with different designated exposure distances and times (i.e., numbers of passes) by the compressed-air plasma jet. In Fig. 8, the oxygen APPJ generates higher concentration of ozone than air APPJ; however, the other reactive nitrogen species (e.g., NO_2) existing in air plasma may also assist the inactivation of bacteria [14]. Yet, it requires further investigation to clarify the roles of these reactive nitrogen species. It was found the compressed-air APPJ treatment can result in very efficient inactivation of both the *E. coli* and *B. subtilis* cells after 10 (residence time: 1.0 s) and 18 passes (residence time: 1.8 s) of exposure, respectively, for all treatment distances (4–20 mm).

Tables 2 and 3 summarizes the survival rates (%) of *E. coli* and *B. subtilis*, respectively, under various test conditions (exposure distance and number of passes). Results clearly show that discharges

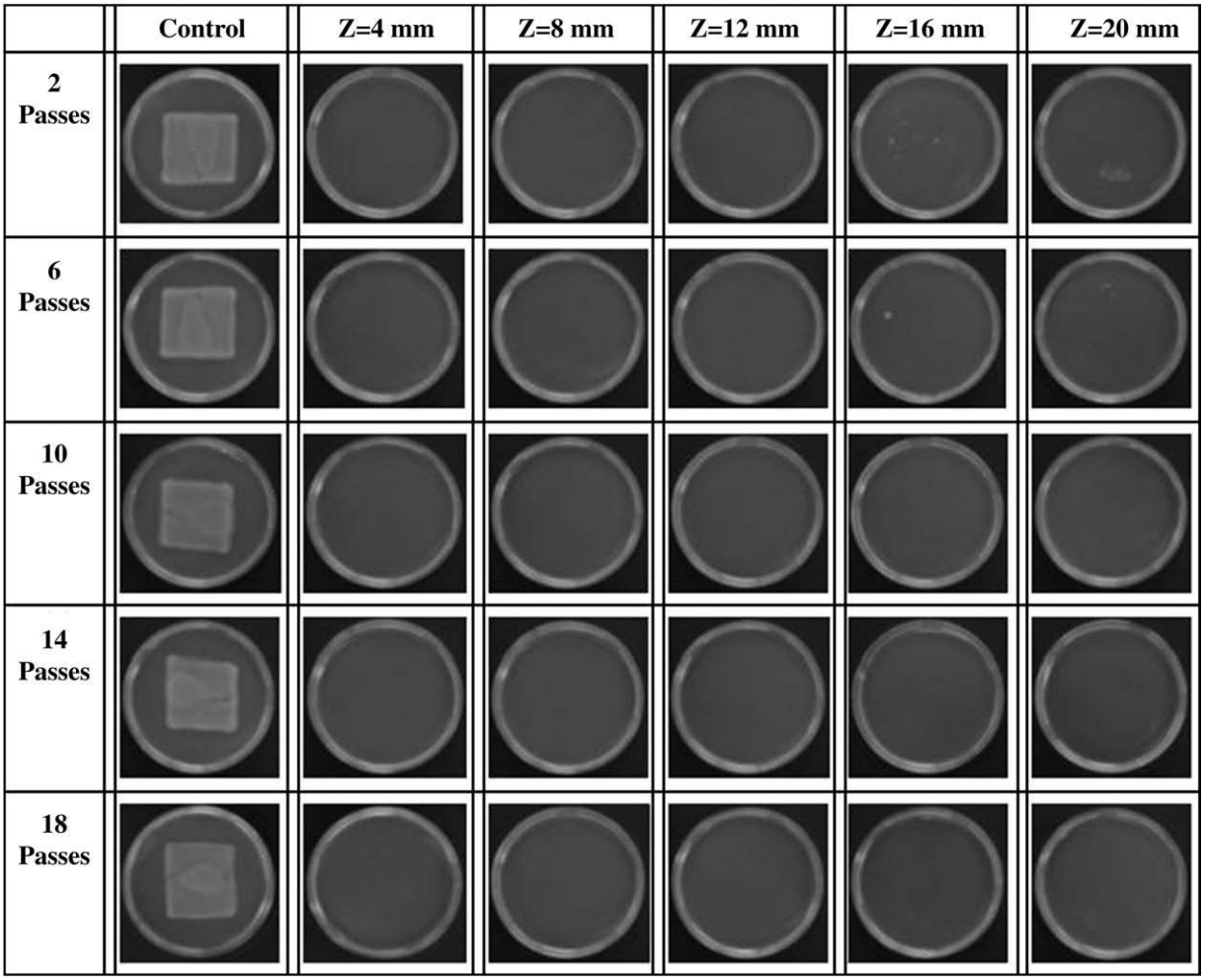

Fig. 9. Appearance of the *E. coli* Petri dish after incubation with different exposure times to different exposure distance and time (number of passes) to compressed-air plasma. Other discharge parameters are: gas flow rate = 10 slm, power = 300 W, and gap = 1 mm.

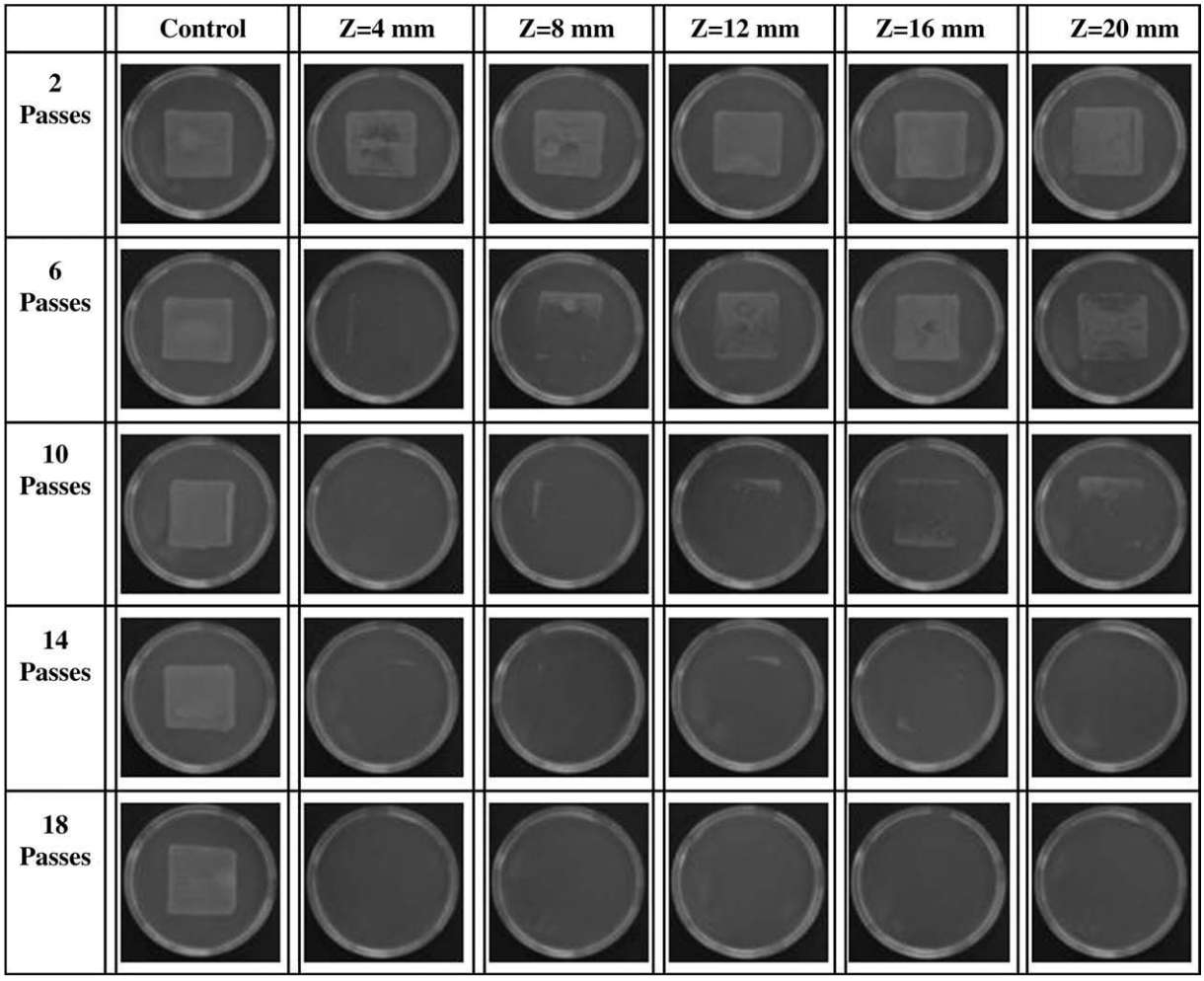

Fig. 10. Appearance of the *B. subtilis* Petri dish after incubation with different exposure distance and time (number of passes) to compressed-air plasma. Other discharge parameters are: gas flow rate = 10 slm, power = 300 W, and gap = 1 mm.

containing oxygen perform excellently in activating both types of bacterial cell because of the existence of oxygen radicals that are very chemically active in reacting with the cells, in which the generation of oxygen radical is explained later.

For *E. coli*, all discharges can totally inactivate the cells within 10 passes of exposure for the highest CFUs ($=10^7$ CFU/mL) except the nitrogen discharge. By using the nitrogen discharge, even after 18 passes of exposure, the inactivation is essentially in vain for the case of 10^7 CFU/mL. The nitrogen discharge possesses much higher germicidal UV emission of NO (180–280 nm) than oxygen and compressed-air discharges, as shown in Fig. 7 earlier. However, the OES measurements have shown that the germicidal UV emission is nearly negligible in the jet region because of quenching from the entrained air and its very short life. This makes the inactivation of the *E. coli* very inefficient as summarized in Table 2. For *B. subtilis*, the results are similar but it generally requires longer period of time (up to 18 passes) of exposure to inactivate the cells for the case of 10^7 CFU/mL. Plasma-generated ozone is at least partially dissociated when immersed into water, liquid-based, or liquid-like biomaterial (bacteria smeared on agar) [15]. Atomic oxygen generated in the process intensively reacts with bioorganic molecules, producing radicals and OH radicals. Thus, the ozone plays an important role in assisting the intensive OH-based biochemical oxidation. It was thought that *B. subtilis* has a thicker peptidoglycan structure (about 20–80 nm) than *E. coli* (about 7–8 nm) [8], which may be the main cause for requiring longer exposure time to inactivate *B. subtilis* cells. Note the

Table 2
Summary of survival rates under different treatment distance for *E. coli* cell (10^7 CFU/mL) on Petri dish for different gas discharge. Other discharge parameters are: gas flow rate = 10 slm, stage moving speed = 1 cm/s, power = 300 W, gap = 1 mm, and $z = 20$ mm.

Working gas	Plasma exposure time (number of passes)	Survival rate (%)
N_2	2/6/10/14/18	94/84/85/95/80
Compressed air	2/6/10/14/18	5/1/0/0/0
O_2	2/6/10/14/18	89/20/3/1/0

Table 3
Summary of survival rates under different treatment distance for *B. subtilis* cell (10^7 CFU/mL) on Petri dish for different gas discharge. Other discharge parameters are: gas flow rate = 10 slm, stage moving speed = 1 cm/s, power = 300 W, gap = 1 mm, and $z = 20$ mm.

Working gas	Plasma exposure time (number of passes)	Survival rate (%)
N_2	2/6/10/14/18	99/94/99/98/97
Compressed air	2/6/10/14/18	88/63/18/0/0
O_2	2/6/10/14/18	80/61/18/3/0

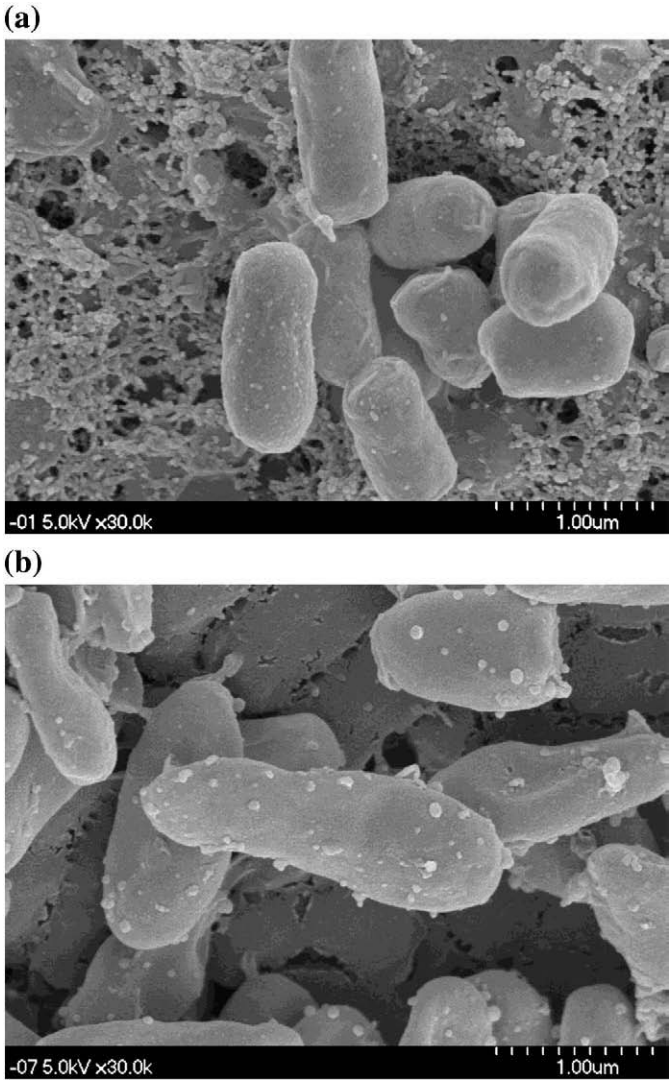

Fig. 11. SEM images of various microorganisms with a parallel-plate DBD APPJ using compressed air: (a) untreated *E. coli* and (b) plasma-treated *E. coli*.

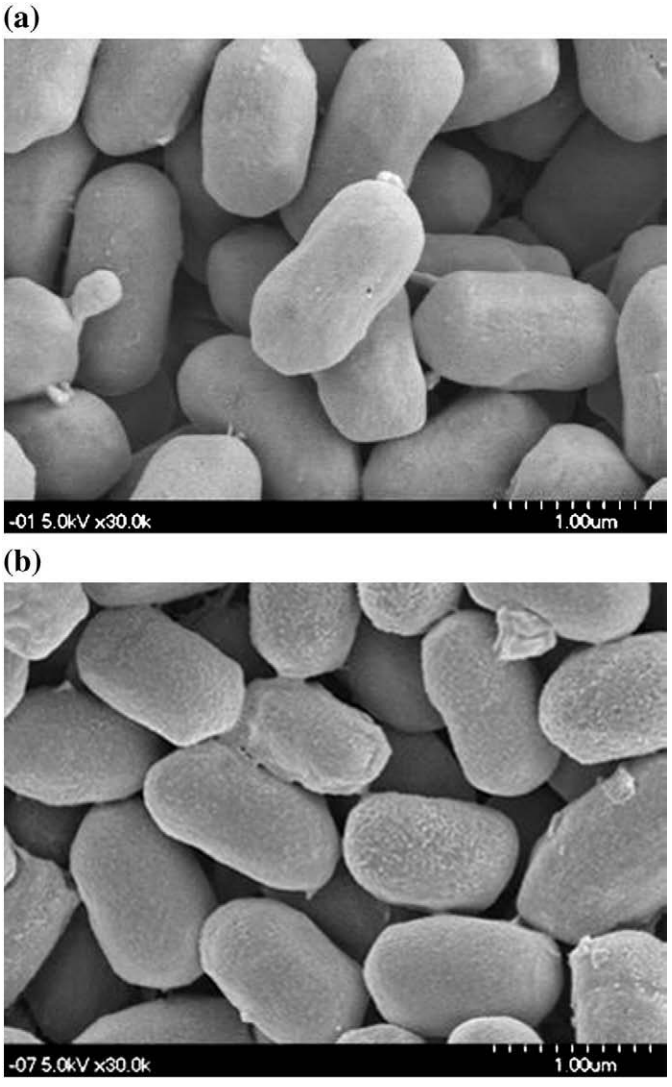

Fig. 12. SEM images of various microorganisms with a parallel-plate DBD APPJ using compressed air: (a) untreated *B. subtilis* and (b) plasma-treated *B. subtilis*.

peptidoglycan exists in periplasmic space between cytoplasmic membrane and outer membrane. The broken peptidoglycan could affect the proper function of solute transportation function for carrying protein in cytoplasmic membrane, which results in effective cell inactivation. Some mechanisms of the inactivation effect on microorganisms by low-temperature plasma have been postulated previously [16]. Nevertheless, the current results show that it is as effective as the previous studies using discharge region by using post-discharge jet region [8,17], which is very encouraging in the viewpoint of application convenience. In addition, considering the cost of operation, the compressed-air discharge may represent the best choice among these.

The SEM images of the untreated and treated *E. coli* and *B. subtils* using compressed-air plasma jet are shown in Figs. 11 and 12, respectively. *Escherichia coli* undergoes some slight morphological change as compared to the control and *B. subtilis* cells was kept nearly intact; however, the bacteria were actually inactivated based on our experimental observation (Tables 2 and 3). This is different from those sterilization studies that showed clear ruptured cell surfaces after plasma treatment. It could be caused by the different plasma doses between the present and other studies. This definitely deserves future investigation (e.g., using bio-TEM) to clarify the underlying cause for the efficient inactivation as found in the current study.

4. Conclusions

In the current study, a parallel-plate DBD APPJ driven by a distorted sinusoidal voltage power supply was characterized electrically by measuring voltage, current and plasma absorbed power, and optically by measuring the OES in the visible–UV regime and absorption spectra in the IR regime. The APPJ was used to inactivate *E. coli* (Gram negative) and *B. subtilis* (Gram positive) up to 10^7 CFU/mL using the post-discharge region. Results show that the post-discharge jet region is very efficient in inactivating these two bacterial cells as previous studies using the discharge region, should the working gas contains appreciable oxygen addition, which in turn generates abundant ozone. In addition, the inactivation is more effective by compressed-air APPJ compared to that by oxygen APPJ, possibly through the assistance of nitrous oxide existing in the former. Major advantage by using post-discharge jet region is its flexibility in practical applications, in which the DBD becomes a stand-alone module that can be used to treat essentially any sample as compared to the conventional applications by using the discharge region.

Acknowledgements

We would like to thank the National Science Council of Taiwan, Institute of Nuclear Energy Research of Taiwan and the Ministry of

Economic Affairs of Taiwan for the financial support through grant nos. 96-2628-E-009-134-MY3, 98I004 and 98-EC-17-A-07-S2-0043 respectively.

References

[1] G.R. Holyoak, S.Q. Wang, Y.H. Liu, T.D. Bunch, Toxicology 108 (1996) 33.
[2] A.D. Lucas, K. Merritt, V.M. Hitchins, T.O. Woods, S.G. NcMamee, D.B. Lyle, S.A. Brown, Inc. J. Biomed. Mater. Res. Part B: Appl. Biomater. 66B (2003) 548.
[3] Y. Wang, T.D. Wig, J. Tang, L.M. Hallberg, J. Food Sci. 68 (2003) 539.
[4] M. Moisan, J. Barbeau, S. Moreau, J. Pelletier, M. Tabrizian, L.H. Yahia, Int. J. Pharmacogn. 226 (2001) 1.
[5] X.T. Deng, J.J. Shi, M.G. Kong, IEEE Trans. Plasma Sci. 34 (2006) 1310.
[6] M. Laroussi, J.P. Richardson, F.C. Dobbs, Appl. Phys. Lett. 81 (2002) 772.
[7] A. Sharma, A. Pruden, O. Stan, G.J. Collins, IEEE Trans. Plasma Sci. 34 (2006) 1290.
[8] Y.Z. Sun, Y.C. Qiu, A.L. Nie, X.D. Wang, IEEE Trans. Plasma Sci. 35 (2007) 1496.
[9] R. Hippler, H. Kersten, M. Schmidt, K.H. Schoenbach, Low Temperature Plasmas: Fundamentals, 2nd Ed., Wiley, New York, 2008, p. 821.
[10] J.B. Sheffield, Microsc. Microanal. 13 (2007) 200.
[11] Y.H. Choi, J.H. Kim, Y.S. Hwang, Thin Solid Films 506–507 (2006) 389.
[12] S.E. Babayan, G. Ding, G.R. Nowling, X. Yang, R.F. Hicks, Plasma Chem. Plasma Process. 22 (2002) 255.
[13] H.E. Wagner, R. Brandenburg, K.V. Kozlov, A. Sonnenfeld, P. Michel, J.F. Behnke, Vacuum 71 (2003) 417.
[14] M. Laroussi, F. Leipold, Int. J. Mass Spectrom. 233 (2004) 81.
[15] A. Fridman, Plasma Chemistry, 1st Ed., Cambridge, New York, 2008, p. 848.
[16] L.F. Gaunt, C.B. Beggs, G.E. Georghiou, IEEE Trans. Plasma Sci. 34 (2006) 1257.
[17] K. Lee, K.H. Paek, W.T. Ju, Y. Lee, J. Microbiol. 44 (2006) 269.